Proceedings of the Seventh International Conference on
Railway Technology: Research, Development and Maintenance
Edited by: J. Pombo
Civil-Comp Conferences, Volume 15, Paper 9.10
Civil-Comp Press, Edinburgh, United Kingdom, 2026
ISSN: 2753-3239, doi: 10.4203/ccc.15.9.10

Mesh Sensitivity Analysis of Xfem-Based Fatigue Crack Investigation in Railway Brake Discs

J. Shen[1,2], J. Zuo[1,2] and Y. Pan[1]

[1]College of Transportation, Tongji University, Shanghai, China
[2]Shanghai Key Laboratory of Rail Infrastructure Durability and System Safety, Tongji University, China

Abstract

This study investigates the mesh sensitivity of an extended finite element method in fatigue crack analysis of railway brake discs, and the stress intensity factor under different crack lengths and mesh sizes is mainly discussed. The results show that the residual stress distribution is nearly mesh-independent, while the calculated stress intensity factor is more sensitive to crack-tip discretization and contour selection. Short cracks exhibit stronger mesh sensitivity and require finer local refinement, whereas longer cracks allow moderately coarser meshes. For the present model, a 1 mm mesh is suitable for 10-20 mm crack lengths, while a 2 mm mesh may be acceptable for longer cracks. The findings suggest that mesh size should be selected according to crack length and stress intensity factor stability rather than using a fixed mesh for all crack cases.

Keywords: railway brake disc, mesh sensitivity, thermomechanical, fatigue crack, stress intensity factor, XFEM.

1 Introduction

Railway brake discs are key safety-related components subjected to repeated thermomechanical loading during braking. The frictional contact between the disc and pad generates transient heat flux, steep temperature gradients, cyclic thermal stresses, and residual stresses on the friction surface. Under severe braking conditions, these effects may lead to thermal fatigue cracking and reduce the structural integrity and service life of the brake disc. Therefore, accurate numerical investigation of thermomechanical fatigue cracks is important for brake disc safety assessment, fatigue life prediction, and maintenance optimization.

Thermal fatigue crack behavior in railway brake discs has been widely investigated from the perspectives of braking conditions, material degradation, residual stress, wear, and crack interaction. Wu et al. [1] developed a thermal crack growth-based fatigue life prediction method for high-speed railway brake discs, linking braking-induced thermal loading with fracture-mechanics-based crack analysis, while Li et al. [2] indicated that braking energy strongly affects fatigue crack propagation. Other studies have examined the effects of different braking conditions on crack behaviour [3-5]. More recent work has further considered thermal expansion, wear, and full thermomechanical coupling effects, showing that contact and wear evolution can influence the temperature and stress fields used for crack assessment [6]. In addition to a single crack, studies on parallel, collinear, and multiple radial cracks manifest that local stress redistribution can significantly affect crack behavior in railway brake discs [7]. These studies provide important background, but they also suggest that a reliable numerical strategy should first be established.

The extended finite element method (XFEM) is an effective approach for crack investigation because it allows cracks to be represented independently of the finite element mesh. Moës et al. [8] introduced the XFEM framework for crack growth without remeshing, and Singh et al. [9] demonstrated its capability in fatigue crack growth simulation and stress intensity factor prediction. XFEM is therefore effective for brake disc crack analysis, especially when cracks are embedded in complex thermomechanical stress fields. However, XFEM results are not completely independent of mesh discretization. Element size, local mesh refinement, crack-tip discretization, enrichment region, and numerical integration may still influence the predicted stress intensity factors, crack-tip response, crack growth tendency, and fatigue-related results [10,11].

Despite existing studies on thermal fatigue cracking, braking-condition effects, wear, residual stress, and crack interaction in railway brake discs, limited attention has been paid to the mesh sensitivity of XFEM-based thermomechanical fatigue crack investigation. This issue is important because an overly coarse mesh may fail to capture steep temperature gradients and crack-tip stress fields, while an excessively fine mesh may lead to unnecessary computational cost. Recent studies on fatigue crack modelling have also emphasized that meshing strategy, computational efficiency, and model validation remain important challenges in numerical crack propagation analysis [12]. A systematic mesh sensitivity analysis is therefore needed to conduct effective crack behavior investigation.

This study aims to perform a mesh sensitivity analysis of XFEM-based thermomechanical fatigue crack investigation in railway brake discs. A finite element model is first established to obtain the transient temperature and stress fields under representative braking conditions. A single crack is then introduced and analyzed using XFEM. Different mesh densities are compared in terms of stress response and stress intensity factor (SIF). The main contribution of this study is to clarify the influence of mesh refinement on XFEM-based crack analysis and to provide practical guidance for reliable and efficient fatigue life evaluation of railway brake discs.

2 Methods

In thermomechanical analysis of the train brake disc, the thermodynamic formulas are mainly used to calculate the temperature and stress fields The three-dimensional temperature field can be described as,

$$\rho C\frac{\partial T}{\partial t}=\lambda\left(\frac{\partial^2 T}{\partial x^2}+\frac{\partial^2 T}{\partial y^2}+\frac{\partial^2 T}{\partial z^2}\right)+\rho Q \tag{1}$$

where ρ , C and λ denote the material's density, specific heat capacity and thermal conductivity, respectively, and Q is the internal heat source intensity. For the railway brake disc, the internal heat source $Q = 0$. Therefore, Eq. (1) can be rewritten as,

$$\frac{\partial T}{\partial t}=\frac{\lambda}{\rho C}\left(\frac{\partial^2 T}{\partial x^2}+\frac{\partial^2 T}{\partial y^2}+\frac{\partial^2 T}{\partial z^2}\right) \tag{2}$$

The temperature gradient can be obtained by the Fourier criterion,

$$\nabla T=-\frac{q}{\lambda} \tag{3}$$

where q includes the absorbed and dissipated heat. The absorbed heat q^{abs} refers to the portion of the heat generated by friction, and the dissipated heat q^{dsp} refers to the heat consumed by convective heat transfer with the ambient air, see Eq.(4),

$$\begin{cases} q^{abs}=\gamma\eta\mu p v=\gamma\eta\mu\dfrac{F}{S}\omega r^{frict} \\ q^{dsp}=\hbar(T^{surf}-T^{amb}) \end{cases} \tag{4}$$

where γ and η represent the energy distribution coefficient and conversion coefficient, μ represents the friction coefficient, p is the normal load, v denotes the linear velocity, F is the braking force, S indicates the effective braking contact area, ω denotes the angular velocity of the brake disc, r^{frict} is the friction radius, $\hbar$ indicates the convective heat transfer coefficient, T^{surf} and T^{amb} represent the temperature on the surface of the material and the ambient air.

In thermodynamics, thermal stress results from temperature change, and the calculation equation is given by Callister [13],

$$\sigma^T=E\alpha(T^{init}-T^{fin})=E\alpha\Delta T \tag{5}$$

where E is the Young's modulus, α indicates the coefficient of thermal expansion, T^{init} and T^{fin} represent initial temperature and final temperature, respectively.

In fracture mechanics, the stress intensity factors can be used to characterize the influence of load or deformation on the stress and strain fields around the crack tips, and to measure the propensity for crack propagation or the crack driving forces. The stress intensity factors of elliptic surface cracks can be formulated as,

$$K_{\mathrm{I}} = F_s\left(\frac{a}{c}, \frac{a}{t}, \frac{c}{W}, \phi\right)\frac{\sigma\sqrt{\pi a}}{E(k)} \tag{6}$$

where ϕ is the crack angle, σ is the stress load, respectively. $E(k)$ is the elliptic integral. F_s represent the geometric correction coefficient, which is related to the geometry of the crack and component, as detailed in Figure 1.

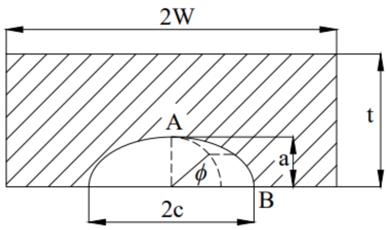

Figure 1: Surface crack.

The extended finite element method (XFEM), a numerical method based on the finite element method (FEM) is widely adopted and applied in crack studies. It is especially designed for treating discontinuities. The XFEM alleviates much of the burden associated with mesh generation by not requiring the finite element mesh to conform to cracks, theoretically [14]. It works by dividing a given domain into two distinct parts, i.e., the mesh generation part (excluding internal boundaries) and the internal boundaries part (enriching the finite element approximation by additional functions) [15,16].

As shown in Figure 2, the grids in the region can be classified into four types, including standard elements, blending elements, split elements, and tip elements. Among them, the split element and tip element are enriched elements, the difference is whether they are crossed by the cracks or not. Besides, blending elements are partially enriched elements, which means that some of their nodes are enriched.

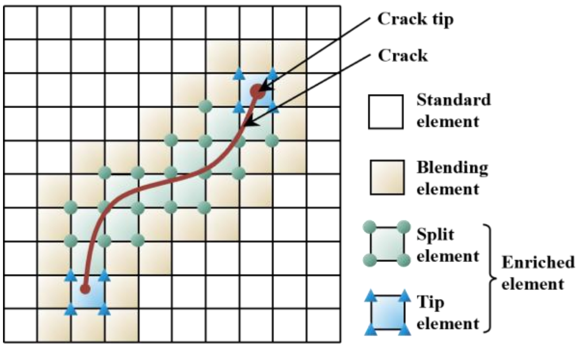

Figure 2: Elements for XFEM.

Therefore, the displacement approximation can be decomposed into the standard part $U^{std}(x)$ and into an enriched part $U^{xfem}(x)$ as,

$$U(x) = U^{std}(x) + U^{xfem}(x) \tag{7}$$

where the enriched part $U^{xfem}(x)$ consists of two parts, one for the split element and one for the tip element, see Eq. (15),

$$U(x) = \sum_{i=1} N_i(x)u^{cont}{}_i + \sum_{j=1} N_j(x)b_i H(x) + \sum_{k=1} N_k(x)\left(\sum_{l=1}^{4} \phi_l\big(r(x),\theta(x)\big)c_k^l\right) \tag{8}$$

where N represents the standard FEM shape function, u^{cont} indicates the displacement approximation of the continuous part of the structure. b and c are unknown enriched degrees of freedom away from and near the crack tip. H denotes the Heaviside enrichment function where the crack crossed. ϕ_l indicates the enrichment function of the crack tip.

3 Results

The brake-disc model used is shown in Figure 3. A sector model of the disc was used, and the mesh was locally refined around the mid-region of the friction surface. This modelling strategy reduces the computational cost, but it also makes the local crack-tip mesh size the key numerical parameter for the extracted SIF.

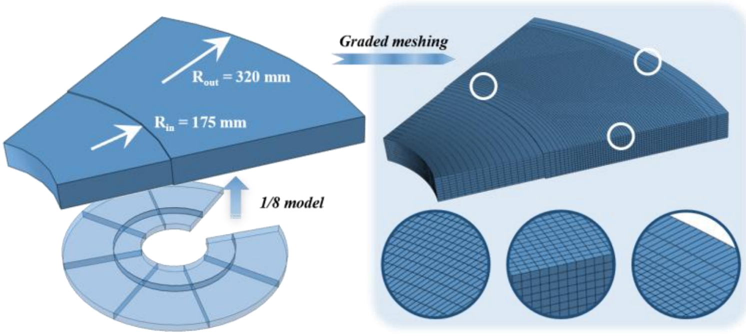

Figure 3: Brake disc model.

The brake disc material's density is 7,751 g·cm^{-3}, and the detailed mechanical properties are shown in Table 1.

Temperature [°C]	Elastic modulus [GPa]	Poisson's ratio	Yield strength [MPa]	Thermal expansion coefficient [10^{-6} K^{-1}]	Thermal conductivity [W·m^{-1}·K^{-1}]	Specific heat [J·kg^{-1}·K^{-1}]
20	211	0.28	1086	10.4	38	524
200	202	0.28	972	11.6	36	575
400	187	0.29	885	13.6	32	607
600	168	0.30	407	14.2	29	752
700	152	0.31	95	14.2	27	840

Table 1: Material properties [17].

The analyzed braking condition is emergency braking with an initial speed of 350 km/h. Figure 4 compares the radial distribution of residual Mises stress obtained under the different mesh conditions. The purpose is to check whether the residual stress, as the driving force for crack propagation, changes with the mesh sizes. The curves in Figure 4 show that the radial residual-stress distribution and its numerical magnitude remain essentially unchanged among the considered mesh conditions.

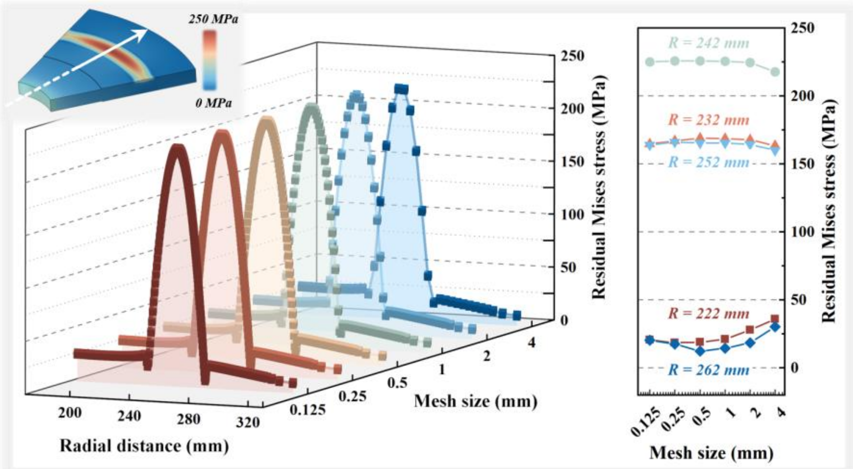

Figure 4: Radial distribution of the residual stress under different mesh conditions.

Since the driving force is not noticeably altered by the mesh size, the differences observed in the SIF results should not be mainly attributed to changes in the residual-stress distribution. Instead, they are associated with the XFEM crack-tip discretization and with the physical size of the contour-integration domains used to extract SIF.

The contour-integral definition used around the crack tip is illustrated in Figure 5. Each contour represents an integration domain surrounding the crack tip, and the contour index increases as the integration domain expands away from the tip.

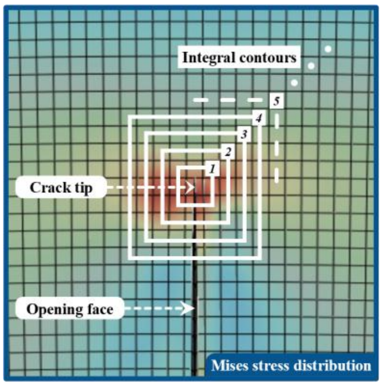

Figure 5: Integral contours around the crack tip.

Figure 6 shows the SIF variation along the contours for the finest mesh size of 0.125 mm. This result demonstrates that the finest mesh does not automatically provide the most reliable SIF. For both the inner tip and the outer tip, the SIF data show that all six crack lengths contain a sign reversal somewhere in the full contour history when mesh size h = 0.125 mm. The sign reversal does not mean that the final SIF must be negative or physically meaningless. Instead, it shows that part of the contour history is path-dependent and should not be selected as the representative SIF. A valid SIF estimate should be taken from a locally stable window. However, this correction has a limitation for very short cracks: for 2c = 2 mm, the stable windows in the current data occur at distances much larger than the crack length itself. Such windows can be numerically smooth but might not be suitable as near-tip extraction regions. In a word, the 0.125 mm mesh reveals the contour sensitivity and shows that over-refinement alone is not a sufficient criterion for choosing the XFEM mesh.

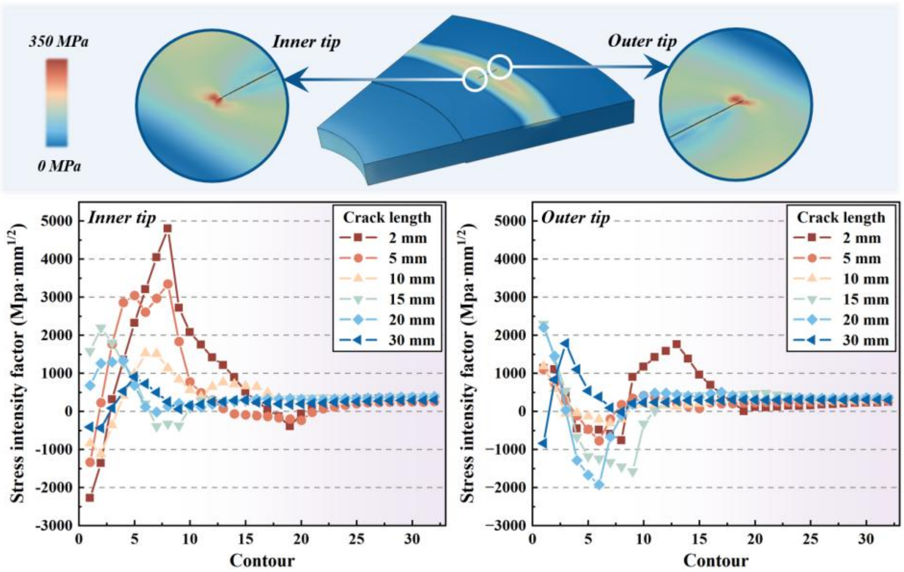

Figure 6: Stress intensity factors of the crack tips, with mesh size h = 0.125 mm.

For varying mesh sizes, the same contour number does not represent the same physical distance when the mesh size changes. For this reason, the SIF results should be interpreted as a function of physical distance from the crack tip, not only as a function of contour number. Figure 7 reorganizes the inner crack tip's SIF results by crack length and plots them against the physical distance from the crack tip. For the outer crack tip, the trend is consistent and therefore not shown. The main result is that the mesh sensitivity is length-dependent. Short cracks are strongly affected by the distance and local contour stability, whereas longer cracks allow the absolute mesh size to be increased once the SIF curve has reached a stable platform.

The shortest crack, 2c = 2 mm, is the most sensitive case. The available stable regions occur only at distances that are large relative to the crack length, and several fine-mesh contour histories show sign changes. Therefore, the current data does not support selecting a final mesh size for the 2 mm crack. This case should be further investigated with a locally refined crack-tip region or with a contour setup that allows a stable platform to appear closer to the crack tip.

For 2c = 5 mm, the data are more usable but still mesh-sensitive. The 1 mm mesh gives SIF = 312.25 MPa mm$^{1/2}$ using the 3rd to 4th contours, while the 0.25 mm mesh gives SIF = 327.55 MPa mm$^{1/2}$ using the 11th to 14th contours. These two values provide a consistent result, but the 0.5 mm mesh gives SIF = 456.40 MPa mm$^{1/2}$ and the coarser meshes are extracted too far from the crack tip. Therefore, the 5 mm crack supports 0.25 mm and 1 mm mesh sizes but still needs further validation.

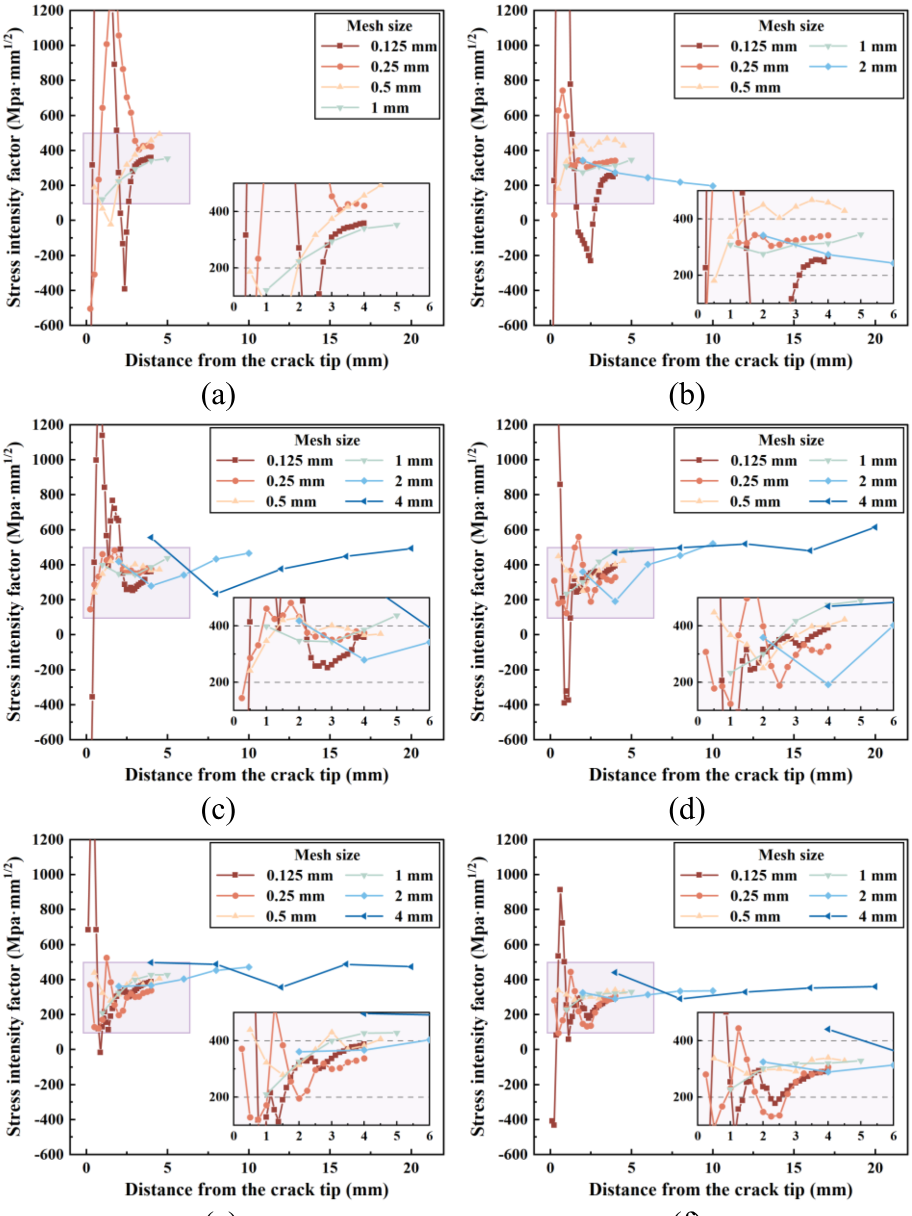

Figure 7: Stress intensity factors of various crack length, (a) 2 mm, (b) 5 mm, (c) 10 mm, (d) 15 mm, (e) 20 mm, (f) 30 mm.

The intermediate crack lengths, 2c = 10-20 mm, show a more regular trend. In this range, the 1 mm mesh gives a balance between stable contour behavior, extraction distance and computational cost. Its representative SIF values are 346.10, 482.25 and 427.55 MPa mm$^{1/2}$ for 2c = 10, 15 and 20 mm, respectively. The selected window is the 2nd to 3rd contours for 2c = 10 mm and the 4th to 5th contours for 2c = 15 and 20 mm. These results support using the 1 mm mesh as the principal mesh size for the 10-20 mm crack range in the current model.

For the longest crack, 2c = 30 mm, the medium mesh sizes give similar SIF levels: 333.63, 320.20 and 335.00 MPa mm$^{1/2}$ for h = 0.5, 1 and 2 mm, respectively. The 2 mm mesh remains close to the finer-mesh results while reducing the modelling cost, and its representative value is taken from the 4th to 5th contours. Therefore, the 2 mm mesh can be selected for efficiency, with the 0.5 mm and 1 mm mesh retained for higher-accuracy verification, the 4 mm mesh could be regarded as a coarse reference.

The overall pattern is therefore not that the smallest mesh is always best. Instead, the admissible absolute mesh size can be increased stepwise as the crack becomes longer. Very short cracks require finer local discretization and stricter contour checking, intermediate cracks in this dataset are adequately represented by a 1 mm mesh, and the 30 mm crack supports a 2 mm mesh when efficiency is required.

The final mesh and contour recommendations are summarized in Table 2. It records the crack-length category, the recommended mesh size, the selected contour with distance range, and the representative inner crack tip's SIF.

Crack length [mm]	Mesh size recommendation [mm]	Selected contour/distance	SIF [MPa $mm^{1/2}$]
2	Further research needed	-	-
5	0.25 mm (for reference)	11th to 14th contours, d = 2.75-3.50 mm; d/2c = 0.55-0.70	327.55
10	1 mm	2nd to 3rd contours, d = 2.00-3.00 mm; d/2c = 0.20-0.30	346.10
15	1 mm	4th to 5th contours, d = 4.00-5.00 mm; d/2c = 0.27-0.33	482.25
20	1 mm	4th to 5th contours, d = 4.00-5.00 mm; d/2c = 0.20-0.25	427.55
30	2 mm	4th to 5th contours, d = 8.00-10.00 mm; d/2c = 0.27-0.33	335.00

Table 2: Summary of the mesh size and corresponding SIF.

4 Conclusions and Contributions

This study investigated the mesh sensitivity of XFEM-based fatigue crack analysis in railway brake discs, focusing on the evaluation of stress intensity factors under different crack lengths and mesh sizes.

The results show that the residual stress distribution is only weakly affected by mesh refinement, so the variation in SIF is mainly related to the XFEM crack-tip discretization and contour selection. Short cracks, especially the 2 mm crack, show strong mesh and contour sensitivity and should be treated with further local refinement and investigation. For medium crack lengths of 10-20 mm, the 1 mm mesh provides a reasonable balance between stability and efficiency in the present results, while for the 30 mm crack, a 2 mm mesh may be acceptable when computational efficiency is considered. Overall, the mesh size can be moderately increased as the crack length increases, but the final choice should still be based on a stable SIF over physically reasonable contours rather than on mesh size alone.

Acknowledgements

The authors would like to appreciate the funding support from the National Natural Science Foundation of China (U25B20233, 62273258) and the Fundamental Research Funds for the Central Universities (22120230311).

References

[1] S.C. Wu, S.Q. Zhang, Z.W. Xu, "Thermal crack growth-based fatigue life prediction due to braking for a high-speed railway brake disc", International Journal of Fatigue, 87, 359-369, 2016.

[2] Z. Li, J. Han, Z. Yang, L. Pan, "The effect of braking energy on the fatigue crack propagation in railway brake discs", Engineering Failure Analysis, 44, 272-284, 2014.

[3] C. Lu, J. Shen, Q. Fu, J. Mo, "Research on radial crack propagation of railway brake disc under emergency braking conditions", Engineering Failure Analysis, 143, 106877, 2023.

[4] H. Zhu, S. Lian, M. Jin, Y. Wang, S. Yang, Q. Lu, Z. Tao, Q. Xiao, "Review of research on the influence of vibration and thermal fatigue crack of brake disc on rail vehicles", Engineering Failure Analysis, 153, 107603, 2023.

[5] J. Shen, C. Lu, J. He, J. Mo, J. Zhao, Z. Hou, "Effect of different braking conditions on fatigue crack propagation behaviour of train brake disc", The Journal of Strain Analysis for Engineering Design, 60(2), 117-130, 2025.

[6] W. Chen, J. Mo, X. Wang, Q. Zhang, W. Jin, C. Zhao, "Thermal crack propagation analysis of railway brake discs considering wear effects via a full thermo-mechanical coupling approach", Wear, 584-585, 206371, 2026.

[7] J. Shen, C. Lu, J. He, J. Mo, J. Zhao, "Interference behavior analysis of parallel cracks on train brake disc using XFEM", Engineering Failure Analysis, 175, 109563, 2025.

[8] N. Moës, J. Dolbow, T. Belytschko, "A finite element method for crack growth without remeshing", International Journal for Numerical Methods in Engineering, 46(1), 131-150, 1999.

[9] I.V. Singh, B.K. Mishra, S. Bhattacharya, R.U. Patil, "The numerical simulation of fatigue crack growth using extended finite element method", International Journal of Fatigue, 36(1), 109-119, 2012.

[10] V.F. González-Albuixech, E. Giner, A. Gravouil, "Analysis of stress intensity factor oscillations in 3D cracks using domain integrals and the extended finite element method", Computer Methods in Applied Mechanics and Engineering, 436, 117739, 2025.

[11] G. Xie, C. Zhao, H. Li, J. Liu, Y. Zhong, W. Du, J. Lv, C. Wu, "An adaptive extended finite element based crack propagation analysis method", Mechanika, 30(1), 74-82, 2024.
[12] A.M. Alshoaibi, Y.A. Fageehi, "Advances in finite element modeling of fatigue crack propagation", Applied Sciences, 14(20), 9297, 2024.
[13] W.D. Callister, D.G. Rethwisch, "Materials science and engineering: an introduction", Wiley, 1964.
[14] N. Sukumar, N. Moës, B. Moran, T. Belytschko, "Extended finite element method for three - dimensional crack modelling", International Journal for Numerical Methods in Engineering, 48(11), 1549-1570, 2000.
[15] H. Pathak, A. Singh, I.V. Singh, S.K. Yadav, "A simple and efficient XFEM approach for 3-D cracks simulations", International Journal of Fracture, 181, 189-208, 2013.
[16] S. Natarajan, C. Song, "Representation of singular fields without asymptotic enrichment in the extended finite element method", International Journal for Numerical Methods in Engineering, 96(13), 813-841, 2013.
[17] C. Yang, Y. Meng, B. Huang, W. Jin, Q. Zhao, B. Wang, Y. Lu, "Simulation of thermal-elastic-plastic cumulative deformation and shaping of brake discs for high-speed trains", Equipment Environmental Engineering, 22(2), 96-104, 2025.